

Isotopic Exchange Study on the Kinetics of Fe Carburization and the Mechanism of the Fischer-Tropsch Reaction

Chai, Jiachun; Pestman, Robert; Chen, Wei; Donkervoet, Noortje; Dugulan, A. Iulian; Men, Zhuowu; Wang, Peng; Hensen, Emiel J.M.

DOI

[10.1021/acscatal.1c05634](https://doi.org/10.1021/acscatal.1c05634)

Publication date

2022

Document Version

Final published version

Published in

ACS Catalysis

Citation (APA)

Chai, J., Pestman, R., Chen, W., Donkervoet, N., Dugulan, A. I., Men, Z., Wang, P., & Hensen, E. J. M. (2022). Isotopic Exchange Study on the Kinetics of Fe Carburization and the Mechanism of the Fischer-Tropsch Reaction. *ACS Catalysis*, 12(5), 2877-2887. <https://doi.org/10.1021/acscatal.1c05634>

Important note

To cite this publication, please use the final published version (if applicable).
Please check the document version above.

Copyright

Other than for strictly personal use, it is not permitted to download, forward or distribute the text or part of it, without the consent of the author(s) and/or copyright holder(s), unless the work is under an open content license such as Creative Commons.

Takedown policy

Please contact us and provide details if you believe this document breaches copyrights.
We will remove access to the work immediately and investigate your claim.

Isotopic Exchange Study on the Kinetics of Fe Carburation and the Mechanism of the Fischer–Tropsch Reaction

Jiachun Chai, Robert Pestman, Wei Chen, Noortje Donkervoet, A. Iulian Dugulan, Zhuowu Men, Peng Wang,* and Emiel J. M. Hensen*



Cite This: *ACS Catal.* 2022, 12, 2877–2887



Read Online

ACCESS |



Metrics & More



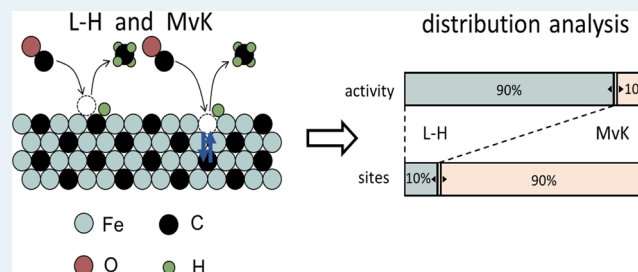
Article Recommendations



Supporting Information

ABSTRACT: The kinetics of the transformation of metallic Fe to the active Fe carbide phase at the start of the Fischer–Tropsch (FT) reaction were studied. The diffusion rates of C atoms going in or out of the lattice were determined using ^{13}C -labeled synthesis gas in combination with measurements of the transient ^{12}C and ^{13}C contents in the carbide by temperature-programmed hydrogenation. In the initial 20 min, C diffuses rapidly into the lattice occupying thermodynamically very stable interstitial sites. The FT reaction starts already during these early stages of carburization. When reaching steady state, the diffusion rates of C in and out of the lattice converge and the FT reaction continues *via* two parallel reaction mechanisms. It appears that the two outer layers of the Fe carbide are involved in hydrocarbon formation *via* a slow Mars–Van Krevelen-like reaction contributing to $\sim 10\%$ of the total activity, while the remainder of the activity stems from a fast Langmuir–Hinshelwood reaction occurring over a minor part of the catalyst surface.

KEYWORDS: Fischer–Tropsch reaction, Fe carbide, carburization, isotopes, mechanism



INTRODUCTION

Since the invention of the Fischer–Tropsch (FT) process, Fe-based catalysts have been studied intensively.¹ They are used in commercial plants by Sasol in South Africa and Shenhua in China,² mainly because of their ability to convert coal-derived synthesis gas with a relatively low H_2/CO ratio. As active Fe catalysts typically contain Fe carbides as well Fe oxides and metallic Fe,³ many studies have dealt with the changes in the catalyst composition during the FT reaction aiming at resolving the nature of the active phase.^{4,5} Nowadays, Fe carbides are generally considered to be the active ingredient of Fe-based FT catalysts.^{6–9} Among these, $\epsilon(\text{'})$ -carbide, $\chi\text{-Fe}_5\text{C}_2$, and $\Theta\text{-Fe}_3\text{C}$ are typically formed under FT process conditions.^{10–13}

Because of their pyrophoric character, Fe carbides are commonly synthesized *in situ* prior to or during the FT reaction. Typically, synthesis gas is used for the conversion of Fe-oxide precursor to Fe carbides. Despite the importance of Fe carbides for the FT reaction, relatively little is known about the kinetics and mechanism of carbide formation. This is especially important when trying to identify correlations between catalyst activation, which mainly involves Fe carburization, and the FT reaction. An early experimental study of Fe carburization relevant to FT synthesis by Niemantsverdriet and Van der Kraan⁶ showed that the FT activity correlated with bulk Fe-carbide formation. It has been widely reported that during catalyst activation, hydrocarbons

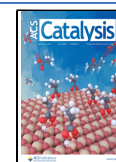
can already be formed. While initially most C derived from CO dissociation is consumed by the carburization process, C hydrogenation to gaseous products becomes more dominant when the bulk of the active phase is saturated by C.¹⁴ Thus, the formation of adsorbed C species by CO dissociation is relevant to both carburization and FT reaction.

Once the active Fe carbide is formed, CH_x intermediates are assumed to be formed on the surface. Chain growth is assumed to proceed *via* the insertion of CH_x monomer into the carbon–metal bond of a growing chain.¹⁵ This mechanism, known as the carbide mechanism, has been proposed by Fischer and Tropsch in 1926¹ and is supported by various experiments.^{16–18} The rupture of a carbon–metal bond in the carbide mechanism shows some similarities to the removal of C from the carbide lattice as occurs in the Mars–Van Krevelen (MvK) mechanism, which has initially been described for oxidation catalysis.¹⁹ In this mechanism, atoms of the surface lattice are directly involved in the catalytic cycle and replenished by reactants from the gas phase. A possible FT reaction path following the MvK mechanism on a C-saturated

Received: December 7, 2021

Revised: January 18, 2022

Published: February 15, 2022



Fe-carbide surface was theoretically proposed by Niemantsverdriet and co-workers.²⁰ Their hypothesis entails the hydrogenation of a lattice carbide C, resulting in the formation of a surface vacancy where a CO molecule from the gas phase can dissociate. This mechanistic cycle is different from the Langmuir–Hinshelwood (L–H) mechanism, in which the reaction occurs between neighboring adsorbed C species and which is normally used to describe the FT reaction on Co and Ru catalysts. Theoretically, both L–H and MvK mechanisms can occur on Fe carbide.

The involvement of C atoms of the carbide surface as reaction intermediates in the FT reaction *via* an MvK mechanism has among others been investigated using isotopic labeling experiments. For instance, Kummer et al.²¹ partially carburized a catalyst with ¹²CO followed by complete carburization with radioactive ¹⁴CO, leading to a ¹⁴C-enriched surface. By carrying out the FT reaction in a ¹²CO/H₂ mixture, it was found that the hydrocarbons produced at 260 °C contained only 10% ¹⁴C as established by measuring their radioactivity. This led to the conclusion that lattice C atoms do not play a major role in hydrocarbons formation. A similar approach was taken by Ordonsky et al.,²² who also found that Fe carbide did not participate appreciably in the FT reaction.

However, all of these studies were performed using catalysts containing a mixture of Fe metal, Fe carbides, and Fe oxides. By solely analyzing the gas-phase composition, the role of each separate iron compound in the FT synthesis cannot be discerned. Hence, it remains elusive if and to which extent C atoms in the FT products originate from the Fe-carbide lattice *via* an MvK mechanism or from adsorbed CO *via* an L–H mechanism. Therefore, a model Raney-Fe catalyst, which contains no oxidic Fe phases, was used in this study. A concomitant advantage of using pure metallic Fe is that the carburization could be studied without the interference of an oxidic Fe phase.²³ Compared to earlier works that only analyzed the gas-phase composition,^{21,22} we also studied changes in the Fe-carbide composition, enabling an accurate demonstration of the existence of any C exchange between lattice and the gas phase. The possible occurrence of either an MvK or an L–H mechanism in the FT reaction was studied by quantifying the occurrence of C exchange followed by comparison of the FT reaction rate with the rates of C diffusing in and out of the carbide lattice, which were determined using ¹³C-labeled synthesis gas in combination with analysis of the transient (labeled) C content of the Fe carbide by temperature-programmed hydrogenation. Subsequently, steady-state transient isotopic kinetic analysis (SSITKA) was used to verify the existence of multiple parallel routes and to determine the corresponding reaction rates.

■ EXPERIMENTAL METHODS

Preparation. Raney-Fe was prepared from an aluminum–iron (Al50/Fe50) alloy (Goodfellow, 150 μm powder). To remove aluminum, 5 g of alloy powder was slowly added to 25 mL of 9 M KOH solution (Sigma-Aldrich) under stirring at 70 °C for 40 min. The suspension was washed with water and ethanol seven times each to remove potassium and aluminum ions and retrieve the Raney-Fe. Leaching aluminum results in a porous structure with a higher surface area than the initial powder. The as-prepared porous Fe powder was transferred into a sealable quartz tube. Due to the pyrophoric character of the fine Fe powder, the catalyst was passivated in a 1% O₂/He flow for 24 h at room temperature for safe handling. According

to ICP-OES (Spectroblue, AMETAK) measurements, the weight composition of the passivated sample was as follows: Fe/Al/O = 85/4/11. Earlier work has shown that Al left behind after Raney-Fe synthesis has no strong influence on Fe carburization.²³ The volume-weighted average size of the passivated Raney-Fe particles was measured on an FEI Tecnai 20 microscope. The average size was 29 ± 2 nm, corresponding, assuming spherical nanoparticles, to a dispersion of 3.5% and a specific surface area of 26.3 m²/g.

Pretreatment and Characterization. The reducibility of the as-prepared Raney-Fe was determined by temperature-programmed hydrogenation (H₂-TPR) using a Micromeritics AutoChem II setup. The sample (30 mg) was loaded into a quartz U-tube between two quartz wool layers. The sample was pretreated at 100 °C for 1 h in a He flow of 50 mL/min before the measurements. The TPR profile was recorded by heating the sample from 40 to 800 °C at the rate of 10 °C/min in a 4 vol % H₂ in a He flow of 50 mL/min.

Ar physisorption (ASAP 2020, Micromeritics) was carried out to determine the surface area of the unsupported precursor and activated catalyst. Typically, 200 mg of sample was treated separately in a sealable reactor, followed by transfer into a sealable measurement tube in a glovebox. Prior to measurements, a reduction was performed at 430 °C in H₂ for 1 h (20% H₂ in Ar, 50 mL/min, 1 bar), followed by carburization at 250 °C in H₂/CO for 40 min (8% CO + 16% H₂ in Ar, 50 mL/min, 1 bar). The surface areas of the passivated, reduced, and carburized samples are 30 ± 6, 31 ± 5, and 29 ± 5 m²/g, respectively. The surface area of the passivated catalyst corresponds to the average particle size determined by TEM analysis. Moreover, these data show that there is no sintering of the Raney-Fe precursor particles during reduction and carburization.

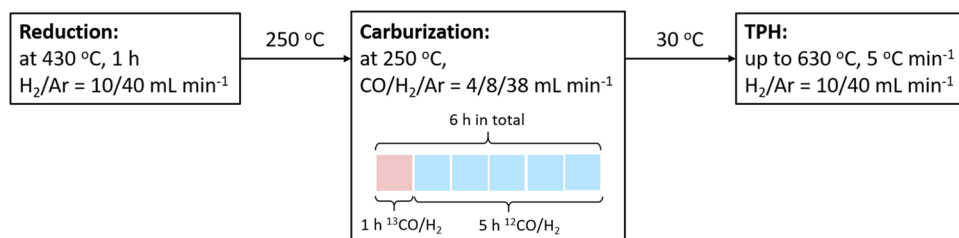
The number of active sites per gram of the catalyst was determined by CO chemisorption (ASAP 2010, Micromeritics). The same pretreatment procedure was applied as for the Ar physisorption measurements. Since it can be expected that part of the surface will still contain adsorbed CO upon carburization, the sample was exposed to a H₂ flow at 250 °C for 10 min (20% H₂ in Ar, 50 mL/min, 1 bar) to remove adsorbed CO. CO chemisorption measurements were conducted at 30 °C. The adsorbed amounts on reduced and carburized catalysts are 0.12 mmol/g and 0.015 mmol/g, respectively. Thus, about 12% of the surface of the carburized sample can adsorb CO.

Transmission ⁵⁷Fe Mössbauer spectra were collected at 120 and 300 K with a sinusoidal velocity spectrometer using a ⁵⁷Co (Rh) source. Velocity calibration was carried out using an α-Fe foil at room temperature. The source and the absorbing samples were kept at the same temperature during the measurements. The Mössbauer spectra were fitted using the Mosswin 4.0 software. Carburization experiments were performed in a high-pressure Mössbauer *in situ* cell. The high-pressure beryllium windows used in this cell contain 0.08% Fe, whose spectral contribution was removed from the final spectra.

Carburization and Isotopic Transient Experiments.

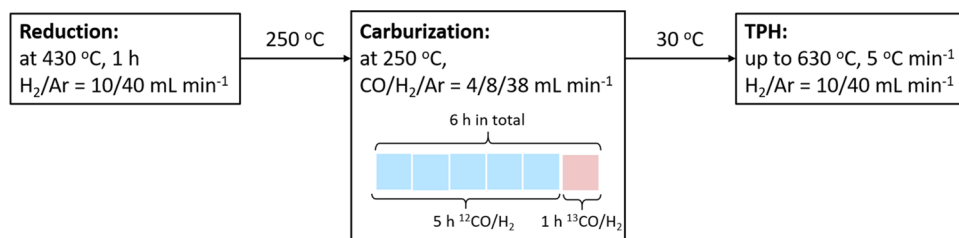
The carburization and FT reactions were studied in a previously described setup,²⁴ in which synthesis gas feeds containing either ¹³CO (99.30% ¹³C, Eurisotop) or ¹²CO (>99.997% with 1.1% ¹³C natural abundance, Linde) could easily be interchanged at constant reaction conditions. For each test, 100 mg Raney-Fe diluted by SiC was loaded. The

Scheme 1. Schematic Representation of the Isotopic Transient Experiment in Which Carburization Is Divided into Blocks of 1 h in either $^{13}\text{CO}/\text{H}_2$ (Pink) or $^{12}\text{CO}/\text{H}_2$ (Blue)^a



^aThe experiments were performed with varying times of $^{12}\text{CO}/\text{H}_2$ exposure (blue blocks) after 1 h exposure to $^{13}\text{CO}/\text{H}_2$ (pink block).

Scheme 2. Schematic Representation of Isotopic Transient Experiment in Which Carburization Is Divided into Blocks of 1 h in either $^{13}\text{CO}/\text{H}_2$ (Pink) or $^{12}\text{CO}/\text{H}_2$ (Blue)^a



^aThe experiments were performed with varying times of $^{12}\text{CO}/\text{H}_2$ exposure (pink blocks) after 1 h exposure to $^{13}\text{CO}/\text{H}_2$ (blue block).

catalyst was first reduced at 430 °C in H_2 for 1 h (20% H_2 in Ar, 50 mL/min, 1.5 bar), followed by cooling to 250 °C and subsequently carburized for varying times in synthesis gas (8% CO + 16% H_2 in Ar, 50 mL/min, 1.5 bar). The gas-phase effluent was analyzed by an online gas chromatograph (GC, Thermo Fischer Scientific Trace GC 1300 equipped with a Trace 1310 Auxiliary Oven). A combination of an MXT-QBond column (60 m \times 0.53 mm) with a thermal conductivity detector was used to determine the concentrations of CO_2 , CO, H_2 and CH_4 , while a combination of an Rt-SilicaBond column (60 m \times 0.32 mm) with a flame ionization detector was used to analyze hydrocarbons.

Temperature-programmed hydrogenation (TPH) performed in the same setup was used to determine the C content of carburized catalysts. After carburization, the catalyst was flushed in Ar and cooled to room temperature. TPH was conducted by heating the reactor to 630 °C at a rate of 5 °C/min in a diluted H_2 flow (20% H_2 in Ar, 50 mL/min, 1.5 bar). During TPH, the main hydrocarbon product was CH_4 (>96%). The CH_4 flow rate was monitored continuously by online MS (ESS CatalySys). A GC taking sample at regular intervals was used to calibrate the MS signal. The carburization degree (C/Fe ratio) was calculated based on the absolute amount of CH_4 evolved during the TPH.

The C exchange of Fe carbide in time was investigated by transient operation, involving switches between $^{13}\text{CO}/\text{H}_2$ and $^{12}\text{CO}/\text{H}_2$ followed by TPH measurements. The protocol for these measurements is shown in Scheme 1. In a first reference experiment, the catalyst was exposed to $^{13}\text{CO}/\text{H}_2$ (8% ^{13}CO + 16% H_2 in Ar, 50 mL/min, 1.5 bar) at 250 °C for 1 h. Afterward, TPH was conducted. Subsequently, the catalyst was exposed to the same treatment with the same labeled synthesis gas mixture for 1 h, followed by a switch to $^{12}\text{CO}/\text{H}_2$ with varying exposure time (1–5 h). The switch between ^{13}C - and ^{12}C -labeled synthesis gas does not chemically alter the reaction because pressure and flow rate were kept the same. Then, a

TPH analysis was applied to determine the C/Fe and $^{12}\text{C}/^{13}\text{C}$ ratios of the carburized samples. The $^{12}\text{C}/^{13}\text{C}$ ratio was determined by online MS. Due to the overlap of signals of fragmented species and the presence of isotopic impurities in the feed gas, the MS signals were corrected by performing reference experiments using only ^{12}CO and ^{13}CO .

To determine the rate of C exchange in Fe carbide, a second set of experiments according to Scheme 2 were performed. In the first set of reference experiments, the catalysts were exposed to $^{12}\text{CO}/\text{H}_2$ (8% ^{12}CO + 16% H_2 in Ar, 50 mL/min, 1.5 bar) at 250 °C for varying times (0.33–5 h). Afterward, TPH was conducted. In subsequent experiments, the catalyst was exposed to the same treatment with unlabeled synthesis gas for varying times, followed by a switch to $^{13}\text{CO}/\text{H}_2$ for 1 h. Again, TPH analysis was employed to determine the C/Fe and $^{12}\text{C}/^{13}\text{C}$ ratios of the carburized samples.

To determine the decarburization rate in Fe carbide, a third set of experiments were performed. The catalyst was first exposed to $^{12}\text{CO}/\text{H}_2$ (8% CO + 16% H_2 in Ar, 50 mL/min, 1.5 bar) at 250 °C for 5 h, followed by a switch to $^{13}\text{CO}/\text{H}_2$ for 1 h. Then, the feed was switched to H_2 (16% H_2 in Ar, 50 mL/min, 1.5 bar) for different times, followed by a TPH measurement to determine C/Fe and $^{12}\text{C}/^{13}\text{C}$ ratios of the decarburized sample.

RESULTS AND DISCUSSION

Carburization Kinetics. The H_2 -TPR profile of as-prepared Raney-Fe contains a single reduction feature at ~ 390 °C (Figure S1). This feature is due to the reduction of the Fe-oxide layer on air-exposed Raney-Fe to metallic Fe. Based on this, a temperature of 430 °C was used for complete reduction of the Raney-Fe precursor in diluted H_2 . Reduced Raney-Fe was carburized and subjected to TPH characterization according to Scheme 1. In Figure 1, we compare three TPH profiles of Raney-Fe carburized according the following protocols (i) 1 h in $^{13}\text{CO}/\text{H}_2$, (ii) 1 h in $^{13}\text{CO}/\text{H}_2$ + 1 h in

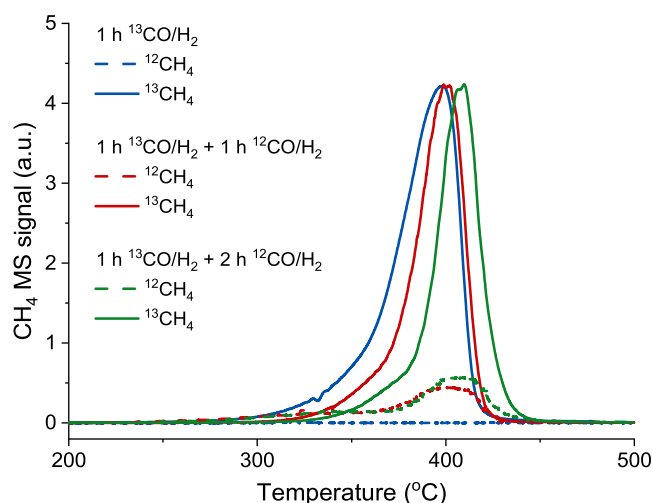


Figure 1. TPH profiles of the samples carburized for 1 h in $^{13}\text{CO}/\text{H}_2$ (blue), carburized for 1 h in $^{13}\text{CO}/\text{H}_2$ followed by $^{12}\text{CO}/\text{H}_2$ for 1 h (red), and carburized for 1 h in $^{13}\text{CO}/\text{H}_2$ followed by $^{12}\text{CO}/\text{H}_2$ for 2 h (green).

$^{12}\text{CO}/\text{H}_2$, and (iii) 1 h in $^{13}\text{CO}/\text{H}_2$ + 2 h in $^{12}\text{CO}/\text{H}_2$. The CH_4 formation peak maximum shifts to a higher temperature with increasing carburization time, pointing to a lower reactivity of C atoms in Fe carbide with increasing carburization degree. Compared to carburization in $^{13}\text{CO}/\text{H}_2$ for 1 h, additional carburization in $^{12}\text{CO}/\text{H}_2$ for 1 and 2 h results in a comparatively small amount of $^{12}\text{CH}_4$. This implies that a high carburization degree is already achieved in the first hour of carburization. The C content of *in situ* formed Fe carbide as determined by TPH is shown in Figure 2. The

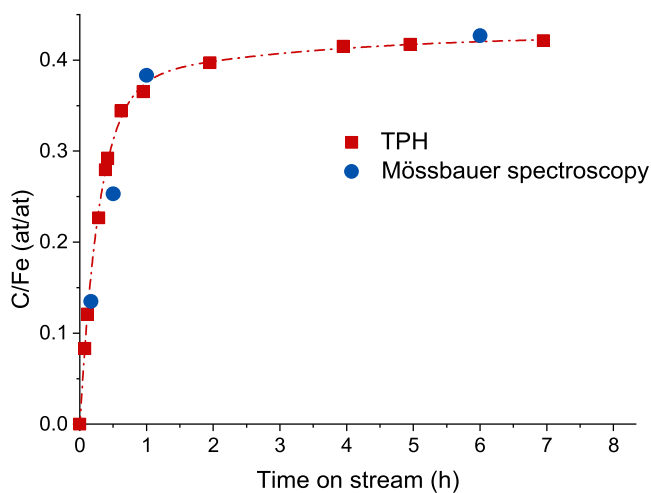


Figure 2. C/Fe ratio of carburized Raney-Fe as a function of carburization time as derived from TPH (red squares) and Mössbauer spectroscopy (blue dots).

evolution of the C/Fe ratio with carburization time is very similar to the results in our previous work.²⁵ We also used Mössbauer spectroscopy to study the phase composition of Raney-Fe as a function of the duration of carburization under similar conditions. Mössbauer spectra were recorded at -153°C to determine the relative contributions of the various Fe species. The resulting spectra are shown in Figure S2, the fit results in Table 1. The excellent agreement between the results

from TPH and Mössbauer spectroscopy demonstrates that TPH is suitable to measure the C content of *in situ* formed Fe carbides.

As shown in Figure 2, the C/Fe ratio is 0.37 after 1 h carburization, corresponding to 88% of the final C/Fe ratio (0.42). While the C/Fe ratio is already 0.4 after 2 h, it takes another 3 h to increase the C/Fe ratio from 0.4 to 0.42. As can be deduced from Table 1, Mössbauer spectroscopy shows that the reduction step preceding the carburization results in the complete reduction of the precursor to metallic Fe. After 10 min carburization, 27% metallic Fe is converted to ϵ' -carbide. After 30 min, 16% χ -carbide and 39% ϵ -carbide are formed. After 6 h, Fe is nearly fully carburized with only 5% metallic Fe (Fe^0) left. This sample contains 70% ϵ' -carbide and 25% χ - Fe_5C_2 . Under these carburization conditions, ϵ' -carbide is more stable than χ - Fe_5C_2 as reported before.²⁵ Notably, no Fe oxides are observed during the carburization process, which indicates that O removal from the surface as either H_2O or CO_2 is fast compared to C removal. In the following, we refer to all ϵ' - and χ - Fe_5C_2 phases collectively as Fe carbides.

Lattice C Exchange. A possible involvement of an MvK mechanism in the FT reaction implies the participation of one or more of the top layers of the catalytic surface in C hydrogenation and coupling reactions. This can be investigated by considering that C vacancies will be occupied by C derived from CO dissociation. We studied the exchange of lattice C by exposure of the Raney-Fe sample to $^{13}\text{CO}/\text{H}_2$ and $^{12}\text{CO}/\text{H}_2$ mixtures for varying times according to Scheme 1, followed by TPH measurements to determine the total amount of C as well as the isotopic $^{12}\text{C}/^{13}\text{C}$ distribution. Figure 3a shows the $^{12}\text{C}/\text{Fe}$ and $^{13}\text{C}/\text{Fe}$ ratios for two experiments involving exposure of Raney-Fe to (i) a $^{13}\text{CO}/\text{H}_2$ mixture for 1 h and (ii) a $^{13}\text{CO}/\text{H}_2$ mixture for 1 h followed by exposure to a $^{12}\text{CO}/\text{H}_2$ mixture for 1 h. By comparing the total C/Fe, $^{12}\text{C}/\text{Fe}$, and $^{13}\text{C}/\text{Fe}$ ratios, we can determine how much C was deposited in the first hour and how much ^{13}C was exchanged in the second hour. In this way, the amount of C removed from the Fe carbide (C_{out}) can be determined, which is defined as the difference between the amount of ^{13}C present in the sample after the original exposure to $^{13}\text{CO}/\text{H}_2$ for 1 h and the amount of ^{13}C left after exposure to $^{12}\text{CO}/\text{H}_2$. C_{net} is the difference between the total amounts of C between the two experiments. C_{in} is the sum of C_{out} and C_{net} and represents the net amount of ^{12}C accumulated during the exposure to $^{12}\text{CO}/\text{H}_2$. In theory, the amount of C exchanged could be higher than determined in this way because the replacement of ^{13}C in carbide by ^{13}CO still present in the gas phase after the switch is not taken into account. The error due to the replacement of the gas phase during the switch is however very low because ^{13}CO gas in the reactor is entirely replaced by ^{12}CO within 5 s after the switch (Figure S3).

Figure 3b shows the results of experiments where an initial exposure to $^{13}\text{CO}/\text{H}_2$ for 1 h was followed by exposure to $^{12}\text{CO}/\text{H}_2$ for longer times. The total C/Fe ratios derived from these experiments agree with those shown in Figure 2. After 2 h carburization, the total C/Fe ratio is 0.4, indicating nearly complete carburization. In the period between 1 and 2 h, the contribution of ^{13}C decreases from 0.37 to 0.34. A rough estimation based on the amount of C exchanged (7%) and the dispersion of Raney-Fe (3.5%) indicates that the first two layers are involved in C exchange events, hinting at the involvement of an MvK-like mechanism. To determine how

Table 1. Mössbauer Fit Parameters of Carburized Raney-Fe Samples^{ab}

sample/treatment	IS (mm/s)	hyperfine field (T)	Γ (mm/s)	phase	spectral contribution (%)	C/Fe
A. Raney-Fe reduction $H_2/Ar = 20/80\%$ 430 °C, 1 h	0.00	33.8	0.35	Fe^0	100	0
B. Raney-Fe carburization $CO/H_2/Ar = 8/16/76\%$ 250 °C, 10 min.	0.00	33.8	0.37	Fe^0	73	0.13
	0.15	26.4	0.72	$\epsilon\text{-}Fe_2C$ (I)	8	
	0.18	18.5	0.72	$\epsilon\text{-}Fe_2C$ (II)	19	
C. Raney-Fe carburization $CO/H_2/Ar = 8/16/76\%$ 250 °C, 30 min.	0.00	33.8	0.33	Fe^0	45	0.25
	0.15	26.4	0.46	$\epsilon\text{-}Fe_2C$ (I)	8	
	0.23	19.0	0.46	$\epsilon\text{-}Fe_2C$ (II)	18	
	0.19	17.7	0.46	$\epsilon'\text{-}Fe_{2.2}C$	13	
	0.21	24.6	0.43	$\chi\text{-}Fe_5C_2$ (I)	8	
	0.17	21.4	0.43	$\chi\text{-}Fe_5C_2$ (II)	5	
	0.18	10.3	0.43	$\chi\text{-}Fe_5C_2$ (III)	3	
D. Raney-Fe Carburization $CO/H_2/Ar = 8/16/76\%$ 250 °C, 1 h	0.00	34.6	0.38	Fe^0	15	0.38
	0.19	27.2	0.41	$\epsilon\text{-}Fe_2C$ (I)	11	
	0.23	19.4	0.41	$\epsilon\text{-}Fe_2C$ (II)	27	
	0.22	18.0	0.41	$\epsilon'\text{-}Fe_{2.2}C$	19	
	0.23	25.1	0.41	$\chi\text{-}Fe_5C_2$ (I)	13	
	0.19	21.3	0.41	$\chi\text{-}Fe_5C_2$ (II)	11	
	0.18	10.3	0.41	$\chi\text{-}Fe_5C_2$ (III)	4	
E. Raney-Fe carburization $CO/H_2/Ar = 8/16/76\%$ 250 °C, 6 h	0.00	33.8	0.30	Fe^0	5	0.43
	0.21	26.1	0.35	$\epsilon\text{-}Fe_2C$ (I)	12	
	0.23	19.3	0.35	$\epsilon\text{-}Fe_2C$ (II)	29	
	0.22	17.7	0.39	$\epsilon'\text{-}Fe_{2.2}C$	29	
	0.23	24.1	0.39	$\chi\text{-}Fe_5C_2$ (I)	12	
	0.17	21.4	0.39	$\chi\text{-}Fe_5C_2$ (II)	9	
	0.18	10.1	0.39	$\chi\text{-}Fe_5C_2$ (III)	4	

^aMössbauer spectra were collected at -153 °C. ^bExperimental uncertainties: isomer shift: I.S. ± 0.02 mm/s; line width: $\Gamma \pm 0.03$ mm/s; hyperfine field: ± 0.1 T; spectral contribution: $\pm 3\%$.

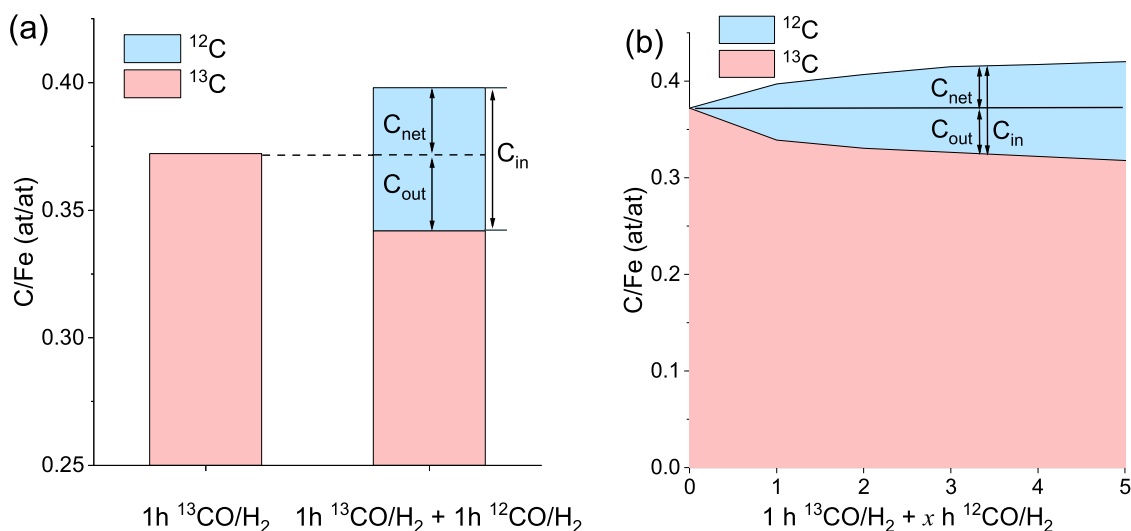


Figure 3. C/Fe ratio of carburized samples. (a) Samples carburized with 1 h $^{13}CO/H_2$ followed by 1 h $^{12}CO/H_2$. (b) Samples carburized with 1 h $^{13}CO/H_2$ followed by x h $^{12}CO/H_2$ (x varies from 0 to 5).

^{13}C was extracted from the carbide, the gas-phase composition was monitored directly after the switch (Figure S3). The instantaneous drop of the ^{13}CO and $^{13}CO_2$ signals in parallel with the inert implies that CO hardly interacts with the carbide and is not responsible for the removal of ^{13}C . On the other hand, the slow decay of the $^{13}CH_4$ signal shows that ^{13}C from the lattice position is removed by hydrogenation to CH_4 .

Prolonging the $^{12}CO/H_2$ carburization time to 5 h yields a nearly fully carburized sample ($C/Fe = 0.42$) and results in a nearly 2-fold increase of the amount of exchanged ^{13}C , evidencing that C atoms deeper into the bulk can be exchanged. Figure 3b shows that the exchange rate slows down with carburization degree but does not vanish. This

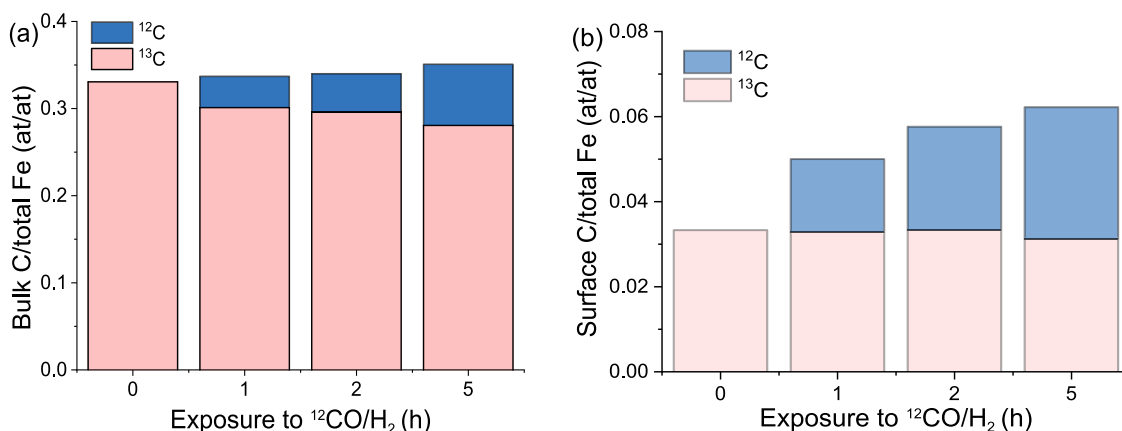


Figure 4. $^{13}\text{C}/\text{Fe}$ and $^{12}\text{C}/\text{Fe}$ distribution in the bulk (a) and surface (b) of Fe carbide as a function of exposure time to $^{12}\text{CO}/\text{H}_2$ following exposure for 1 h to $^{13}\text{CO}/\text{H}_2$.

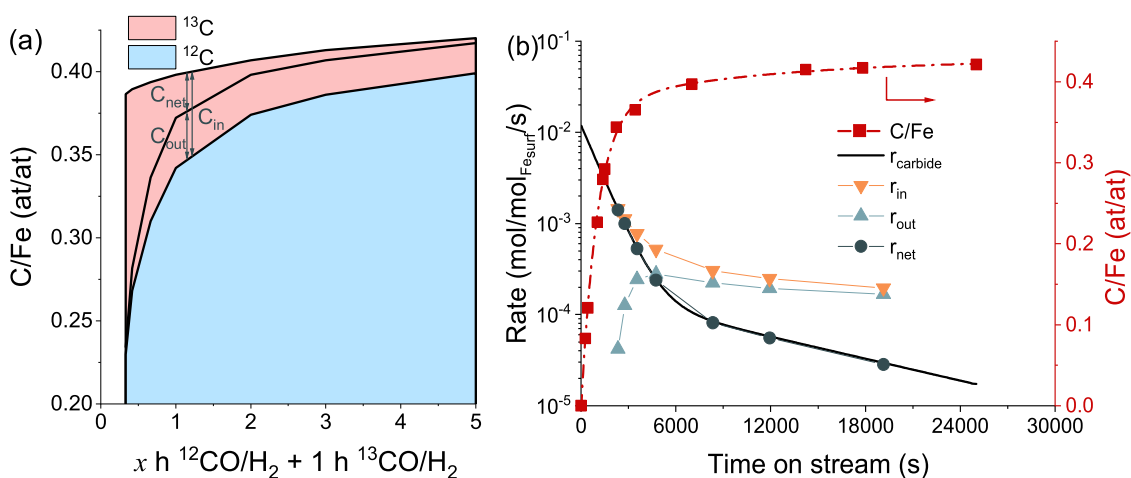


Figure 5. Isotope composition change and carburization rates of experiments following Scheme 2: carburization by $^{12}\text{CO}/\text{H}_2$ for varying times, followed by 1 h $^{13}\text{CO}/\text{H}_2$: (a) the isotope composition, represented by the colored areas and the C/Fe ratio after $^{12}\text{CO}/\text{H}_2$ exposure only (middle black line). (b) Evolution of total C/Fe ratio (squares), carbide formation rate based on the derivative of the C/Fe ratio (black curve), carbon entering rate (downward triangles), carbon leaving rate (upward triangles), and the net accumulation rate r_{net} (circles) as a function of time on stream in the carburization process (8% $\text{CO} + 16\% \text{H}_2$, 250 °C).

points to a slow but continuous involvement of C atoms of the Fe carbide in the FT reaction *via* an MvK mechanism.

Mössbauer spectroscopy can be used to determine the overall C/Fe ratio based on the relative contributions of the main bulk Fe-carbide phases. The C/Fe ratio can also be determined by TPH analysis. It can be expected that the C/Fe ratio determined by TPH is higher than the ratio determined by Mössbauer spectroscopy because the former technique also titrates surface adsorbed carbonaceous species. The close agreement between the two methods indicates that the contribution of surface adsorbed species to the overall C/Fe ratio is minor. Adsorbed species can play a role in the exchange of C atoms from the bulk Fe carbide with the gas phase. To understand this aspect in more detail, the TPH profiles were deconvoluted into separate contributions for surface C and bulk C. This is possible because during TPH different carbon-containing intermediates are hydrogenated at specific temperatures, *viz.*, in order of decreasing reactivity (i) adsorbed carbon-containing species and surface carbide, (ii) bulk C, and (iii) graphitic C.²⁶ The TPH results present contain distinct features. The one observed at the lowest temperature is ascribed to surface C species, while the second feature in the

range between 380 and 480 °C can be related to bulk C, which includes all lattice C atoms in the inner layers of the Fe carbide. The absence of a clear peak above 500 °C indicates that there is not much graphitic C present. The TPH profiles of $^{12}\text{CH}_4$ and $^{13}\text{CH}_4$ for an experiment involving varying $^{12}\text{CO}/\text{H}_2$ exposure times (1–5 h) after a preceding 1 h $^{13}\text{CO}/\text{H}_2$ carburization step are displayed in Figure S4. As expected, the increase in the amount of $^{12}\text{CH}_4$ with reaction time (Figure S4a) goes at the expense of the amount $^{13}\text{CH}_4$ (Figure S4b), consistent with an MvK mechanism. To distinguish the contribution of surface C and bulk C in the C exchange, the TPH profiles of $^{12}\text{CH}_4$ and $^{13}\text{CH}_4$ were deconvoluted (Figure S5). The profiles of the experiments involving 0 and 1 h of exposure to $^{12}\text{CO}/\text{H}_2$ could be fitted by two features that are due to hydrogenation of surface and bulk C species. Prolonged exposure to $^{12}\text{CO}/\text{H}_2$ required fitting with three peaks, namely, surface C and two bulk C features, the latter two denoted by C_1 and C_2 . The nature of these two bulk carbide species remains unknown. We tentatively ascribe C_1 to a Fe carbide that features moderate hydrogenation ability and the smaller C_2 peak to Fe carbide whose hydrogenation is hindered by oligomeric C or a very small amount of graphitic C.

Figure 4 summarizes the results of the TPH analyses in which the ^{12}C and ^{13}C contributions to bulk C (Figure 4a) and surface C (Figure 4b) of the Fe carbide are differentiated. The amount of bulk ^{13}C declines with prolonged ^{12}CO exposure, implying that C from the carbide lattice can be exchanged. Simultaneously, the contribution of bulk ^{12}C gradually increases as more ^{12}C from the gas phase enters the bulk of Fe carbide. As the total amount of bulk C also increases, ^{12}C does not only replace ^{13}C but also increases the C content of the Fe carbide. It should be noted that ^{13}C atoms that are exchanged by ^{12}C leave the bulk by passing through the surface layer. Figure 4b displays the isotopic composition of the surface C layer. ^{12}C is built up on the surface when the sample is exposed longer to ^{12}CO . This points to the accumulation of surface C species. The nearly constant ^{13}C content of the surface suggests that the surface C species formed during the first hour of exposure to ^{13}CO are replenished by ^{13}C from the bulk. These observations highlight the dynamic behavior of C both at the surface and in the bulk of Fe carbide. Contrary to the theory that anticipates bulk C is a spectator in the FT reaction,²⁷ our results strongly indicate surface C can be supplied by the outward diffusion of bulk C.

C Exchange and Diffusion Rates. The experiments presented in Figures 3 and 4a reveal that C atoms from the carbide bulk can be exchanged by C atoms from gas-phase CO. However, no detailed information about the rate of this exchange is obtained from these experiments. Therefore, we set up another series of experiments, where the catalysts were first treated in $^{12}\text{CO}/\text{H}_2$ for periods of 0.33–5 h followed by exposure to $^{13}\text{CO}/\text{H}_2$ for 1 h (Scheme 2). For comparison, the catalysts were also only treated in $^{12}\text{CO}/\text{H}_2$ for the same periods without subsequent exposure to the labeled synthesis gas mixture. The total C/Fe ratios determined by TPH before as well as after 1 h exposure to $^{13}\text{CO}/\text{H}_2$ are shown in Figure 5a. The reaction rate of lattice C atoms leaving and entering the catalyst in 1 h, respectively, denoted as r_{out} and r_{in} , can now be derived by dividing the amounts C_{in} and C_{out} by the exposure time to $^{13}\text{CO}/\text{H}_2$ (1 h). Figure 5b shows the difference between these two rates, which is the net carburization rate (r_{net}), as a function of the $^{12}\text{CO}/\text{H}_2$ carburization treatment. The figure also includes the evolution of the total C/Fe ratio. The carbide formation rate based on the derivative of the total C content as a function of carburization time is also shown in Figure 5b and matches well the values of r_{net} derived from the isotopic measurements. r_{in} decreases rapidly with time on stream from the very beginning. At the same time, r_{out} slowly increases. After about 6 h, an equilibrium is reached where r_{in} and r_{out} converge to the same value, representing the stage that the catalyst attains its final C/Fe ratio under the given conditions. The fact that r_{in} is much higher than r_{out} at the early stage of carburization indicates that, at this stage, practically all C atoms entering the catalyst migrate to the lattice position. This inhibits C exchange reactions. At later stages of the carburization process, r_{in} and r_{out} converge expectedly.

To better understand the early stages of carburization, additional experiments were performed at a shorter time scale. For this purpose, the catalyst was carburized for only 20 min by $^{13}\text{CO}/\text{H}_2$ preceding a switch to $^{12}\text{CO}/\text{H}_2$. The results presented in Figure S6 show that C atoms entering the catalyst during the initial 20 min cannot be replaced by C atoms entering later, even after extending the exposure time to 100 min. Clearly, the C atoms entering the fresh Fe catalyst in the

first 20 min (about 50% of the saturated C concentration in Fe carbide) are bound very tightly to the lattice. This contrasts with the results shown in Figure 3, which show that, after 1 h carburization, nearly 85% of the maximum C/Fe ratio is reached. About 7% of these C atoms, which is equivalent to the first two layers, can be exchanged during the following 1 h exposure to $^{12}\text{CO}/\text{H}_2$. After 6 h carburization when the catalyst is fully carburized, approximately 5% C can be exchanged within 1 h (Figure 5b). In conclusion, all of the C atoms that diffuse into the Fe in the first 20 min cannot be exchanged. This suggests that C diffuses to energetically stable interstitial sites. C atoms entering at a later stage occupy less stable positions, allowing for facile exchange.

To study the decarburization rate, the following transient experiment was performed: a reduced Fe catalyst was fully carburized in $^{12}\text{CO}/\text{H}_2$ for 5 h, followed by a 1 h treatment with $^{13}\text{CO}/\text{H}_2$. TPH analysis showed that the carburized catalyst contained 95% ^{12}C and 5% ^{13}C . As the last hour of carburization was conducted in $^{13}\text{CO}/\text{H}_2$, it can be expected that the ^{13}C atoms predominantly reside in the top layers, while the ^{12}C sits atoms mostly occupy the bulk. This is confirmed by $^{13}\text{CH}_4$ and $^{12}\text{CH}_4$ TPH analyses shown in Figure S7. After 6 h carburization, an abrupt switch was made to a flow containing only H_2 . The remaining amounts of ^{12}C and ^{13}C in the Fe carbide were followed in time by TPH analysis. The respective decarburization rates were determined by calculating the derivatives of the ^{12}C , ^{13}C , and total C amounts as a function of decarburization time. The resulting rates are presented in Figure 6 together with the decay in the total C/Fe

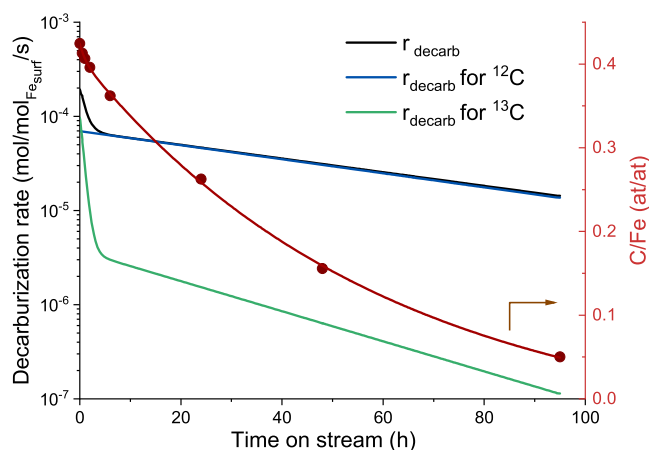


Figure 6. Decarburization rate as a function of time on stream in a reaction with H_2 (16% H_2 , 250 °C, 1.5 bar) of a catalyst carburized in $^{12}\text{CO}/\text{H}_2$ for 5 h followed by 1 h exposure to $^{13}\text{CO}/\text{H}_2$: decarburization rate of ^{12}C (blue curve) and ^{13}C (pink curve) and the overall decarburization rate (black curve). The total C content expressed as the atomic C/Fe ratio is provided as well (brown curve).

ratio. Notably, the initial overall decarburization rate at the start of the decarburization is approximately equal to r_{out} at the end of the carburization experiment shown in Figure 5b, amounting to 1.8×10^{-4} mol C/mol $\text{Fe}_{\text{surface}} \text{ s}^{-1}$. Both rates represent the rate of C removal after 6 h carburization. Even though the rates are obtained in different gas atmospheres, they are nearly equal, which suggests that the rate-limiting step in the decarburization process is independent of the gas-phase composition and, consequently, the surface coverage. A possible explanation for this is that the slow step in the

overall decarburization process is the migration of C from interstitial sites to sites close to the surface. It takes 95 h to remove 86% of the C in the carbide, while introducing this amount of C in reduced Raney-Fe at the same temperature takes only 1 h. This difference reflects the high thermodynamic stability of C in the Fe-carbide lattice, leading to a lower overall activation barrier for carburization than for the reverse decarburization process. It should be noted that, to take part in the FT reaction *via* an MvK mechanism, a C atom has to leave the Fe-carbide lattice. As can be seen in Figure 6, the overall decarburization rate slows quickly at the start and gradually afterward. The high rate at the beginning can be ascribed to the fast removal of ^{13}C atoms that are located in the outermost layers of the Fe-carbide particles. After the fast decay, the overall C removal rate overlaps completely with the ^{12}C removal rate. Thus, after the ^{13}C -containing top layers were removed, the remaining ^{12}C atoms diffuse slowly to the surface to complete the decarburization process.

Comparison with FT Rates. As the carburization reaction studied above competes with hydrocarbons formation from the same surface C species, it is useful to compare these two reactions by following how they change directly after exposure to synthesis gas. The carburization rate as calculated by the derivative of the total C content as a function of carburization time and the C_xH_y formation rates are plotted in Figure 7. The

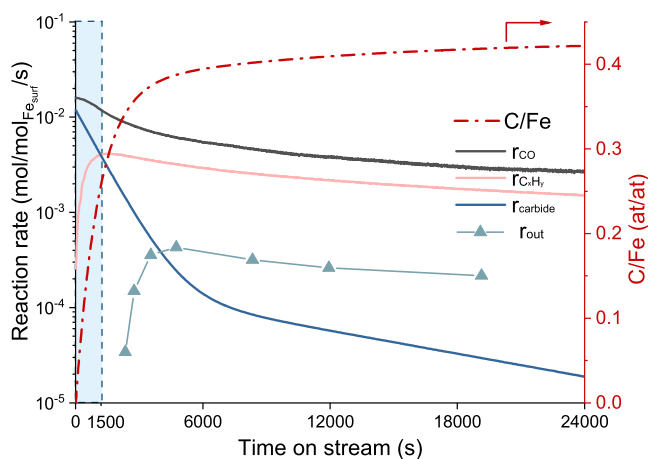


Figure 7. CO consumption rate, carbide formation rate, C_xH_y formation rate, r_{out} , and the C/Fe ratio as a function of time on stream at 250 °C, 1.5 bar, $\text{H}_2/\text{CO} = 2$ (note that r_{out} and the carbide formation rate are taken from Figure 5).

latter carbon-based rate is determined on the basis of all analyzed hydrocarbons ($\text{C}_1\text{--C}_{10}$). The reaction was started by switching from H_2 to CO/H_2 . Carbide formation, which starts immediately and is the dominant reaction in the early stages of carburization, slows with increasing C/Fe ratio. By contrast, the rate of C_xH_y formation rate goes up as the carburization degree increases. The C_xH_y formation rate reaches a maximum after *ca.* 1500 s, when the C/Fe ratio is 0.3. This corresponds to a carburization degree of 72%. Qualitatively, these trends can be explained by variations in the Fe–C bond energy as a function of the C/Fe ratio of the active phase. The initial reduced Fe phase has a very strong affinity for C,²⁸ which can explain the preferential diffusion of the C atoms into the Fe lattice over their hydrogenation. The average Fe–C bond energy in the bulk and at the surface will decrease with increasing C/Fe ratio.²⁹ A lower Fe–C bond energy favors

hydrocarbons formation and lowers the rate of carburization. The latter rate also decreases with increasing C/Fe content because less lattice sites are available.

After 80 min, about 10% of the C atoms in C_xH_y formation come from Fe carbide (r_{out}). This result is in qualitative agreement with the study by Kummer et al.²¹ These authors observed a radioactive ^{14}C content of $\sim 10\%$ among hydrocarbon products during the FT reaction with $^{12}\text{CO}/\text{H}_2$ at 260 °C after carburization in a $^{14}\text{CO}/\text{H}_2$ mixture. This result confirms that C exchange *via* an MvK-like mechanism takes place and contributes to the overall FT activity. The major FT pathway responsible for the remaining 90% of the FT activity is likely a parallel L–H pathway involving surface adsorbed intermediates. Thus, it is interesting to study the role of these two reactions in more detail by steady-state transient isotopic kinetic analysis (SSITKA), as this technique allows estimating the rates and relative contributions of parallel reaction pathways.³⁰

Parallel Reaction Pathways. SSITKA was performed by switching from $^{12}\text{CO}/\text{H}_2$ to $^{13}\text{CO}/\text{H}_2$ after 5 h carburization ($\text{H}_2/\text{CO} = 2$). The response of the reaction products was followed by online MS. Interpretation of such SSITKA measurements is usually based on the assumption that the reaction occurs on the catalytic surface *via* an L–H mechanism. When considering a contribution of an MvK mechanism, parameters like residence time and surface coverage become less meaningful. Nevertheless, the transient response of the products still bears important kinetic information. The usual approach is to describe the evolution of the simplest hydrocarbon CH_4 by a pseudo-first-order process.^{31–33} In this way, kinetic information about parallel reaction pathways can be obtained.^{31,33,34} Details of the data modeling are provided in the Supporting Information. A reasonable fit was obtained involving 4 pools of active sites, each exhibiting a different activity (Table S1). Table 2 lists for

Table 2. Modeling of SSITKA CH_4 Response with Four Pseudo-First-Order Reaction Rate Constants with x_i the Fractional Contribution to the Total CH_4 Rate and y_i the Fraction Contribution to the Total Number of Active Sites

pathway i	rate constant k_i (s^{-1})	x_i (%)	y_i (%)
1	3.23×10^{-4}	16.5	89.8
2	4.23×10^{-3}	19.9	8.2
3	2.15×10^{-2}	20.8	1.7
4	2.76×10^{-1}	41.3	0.2

each of these pools the fitted pseudo-first-order rate constant k_i , the corresponding fractional contribution x_i to the total reaction rate, and the fractional contribution y_i to the total number of active sites. The rate constants span several orders of magnitude ranging from 3.2×10^{-4} to $2.8 \times 10^{-1} \text{ s}^{-1}$. The most abundant active sites have a rate of $3.2 \times 10^{-4} \text{ s}^{-1}$, representing 89% of the total amount of active sites and contributing 17% to the total rate. Note that the fitted rate constant of this slow reaction path is in the same range as the experimentally observed exchange rate of C atoms in the Fe-carbide catalyst in steady state, *i.e.*, $2 \times 10^{-4} \text{ s}^{-1}$ (Figure 5, for $r_{\text{out}} = r_{\text{in}}$). We tentatively attribute this relatively slow reaction pathway to CH_4 formation *via* an MvK mechanism, which involves the difficult extraction of C from the surface lattice. This assumption is consistent with the result from Figure 7 that the rate of C removal from the lattice is around 10% of the

C_xH_y formation rate. The other faster pathways occupy together about 10% of the surface area but have a much larger contribution to the total activity. According to CO chemisorption, only 12% of the surface Fe sites is accessible for adsorption. Hence, we suggest that the fast reaction pathways can be associated with L–H reactions involving adsorbed C species on Fe sites. The proposed assignment of MvK and L–H reaction mechanisms to slow and fast reaction pathways fits with the notion that extraction of C from the carbide is slower than reactions between adsorbed species. The existence of multiple L–H reactions with different rates could be due to the presence of more than one active site on the Fe-carbide nanoparticles. Overall, these data show that the CH_4 activity over Fe carbide is dominated by a reaction path following the L–H mechanism with a small contribution of an MvK mechanism. The existence of more than one pool of C atoms (C_a and C_b) in CH_4 formation on Fe-based FT catalysts was already proposed by Govender et al.³⁰ They also pointed out that a slow pool (C_a) makes a small contribution to the total activity but takes up most of the surface. Their kinetic analysis did however not reveal the origin of the C pools. In another study by Graf et al., the possibility of multiple pools was mentioned but not linked to specific reaction routes.³⁵ The transient kinetic analysis in this work deals exclusively with CH_4 formation. This implies that we cannot draw conclusions about the impact of C exchange on the formation of hydrocarbons with more than one C atom. It is however worthwhile to point out that it has been shown that C–C coupling reactions involve both fast and slow C pools,^{30,36} suggesting that the current results would also be relevant to the FT reaction. Ordonsky et al. found that labeled C atoms in Fe carbide are only involved in the chain growth initiation events of the FT reaction.²² Based on this insight, it can be speculated that the slow C pool, which involves lattice C, provides the CH_x species for chain growth initiation *via* an MvK mechanism while the fast C pool provides chain growth monomers by CO hydrogenation *via* an L–H mechanism occurring on a small fraction of the total surface area. It cannot be excluded that CH_x species obtained by hydrogenation of surface carbide C atoms migrate to other sites where they are involved in L–H-type reactions that give rise to higher hydrocarbons. In any case, the small contribution of surface carbide C atoms must stem from the relatively strong binding to Fe compared to adsorbed C atoms.

CONCLUSIONS

Iron carburization of a fully metallic Fe catalyst and the FT reaction mechanism were studied with alternating unlabeled and ^{13}C -labeled synthesis gas streams. By analyzing the transient change in labeled C composition of the carbide over time, not only the carburization rate but also the diffusion rate of C entering and leaving the carbide could be determined. Initially, carburization dominates over hydrocarbon formation because of the high stability of C atoms in the Fe lattice. After about 20 min, half of the maximum C/Fe ratio was obtained. The C atoms dissolved during this stage can hardly be exchanged. After 6 h, the rates of C leaving and entering the carbide converge, indicating that maximum carburization is obtained. At this steady state, a limited amount of C atoms representing roughly the two outermost layers of the Fe-carbide particles can be exchanged and about 10% of the total FT activity is attributed to this C diffusing out of the carbide. An SSITKA measurement involving a switch of $^{13}CO/H_2$ to

$^{13}CO/H_2$ over a completely carburized catalyst points to the existence of four parallel reaction paths expanding several orders in rate for CH_4 formation. The slowest reaction path occurs on the largest fraction of the surface and its rate has the same order of magnitude as the rate at which C diffuses out of the lattice during the steady state. The fast reaction path dominates the CH_4 formation rate but runs over only about 10% of the catalyst surface which coincides with the percentage of CO adsorption sites. In contrast to the previous literature, which does not link reaction rates to mechanisms nor reaction sites, it can thus be proposed that the slow path corresponds to a C hydrogenation pathway *via* an MvK mechanism and that the dominant fast pathway involving only a small part of the surface can be attributed to CO hydrogenation *via* an L–H mechanism.

ASSOCIATED CONTENT

Supporting Information

The Supporting Information is available free of charge at <https://pubs.acs.org/doi/10.1021/acscatal.1c05634>.

H_2 -TPR profile; Mössbauer spectroscopy; transient response of gases after a switch from $^{13}CO/H_2$ to $^{12}CO/H_2$; TPH profiles; deconvolution of TPH profiles; and C/Fe ratio as a function of reaction time in $^{12}CO/H_2$ (Section I) and SSITKA data analysis (Section II) (PDF)

AUTHOR INFORMATION

Corresponding Authors

Peng Wang – Laboratory of Inorganic Materials Chemistry, Schuit Institute of Catalysis, Department of Chemical Engineering and Chemistry, Eindhoven University of Technology, 5600 MB Eindhoven, Netherlands; National Institute of Clean-and-Low-Carbon Energy, Future Science and Technology City, Beijing 102211, People's Republic of China; Email: peng.wang.hm@chnenergy.com.cn

Emiel J. M. Hensen – Laboratory of Inorganic Materials Chemistry, Schuit Institute of Catalysis, Department of Chemical Engineering and Chemistry, Eindhoven University of Technology, 5600 MB Eindhoven, Netherlands; orcid.org/0000-0002-9754-2417; Email: e.j.m.hensen@tue.nl

Authors

Jiachun Chai – Laboratory of Inorganic Materials Chemistry, Schuit Institute of Catalysis, Department of Chemical Engineering and Chemistry, Eindhoven University of Technology, 5600 MB Eindhoven, Netherlands

Robert Pestman – Laboratory of Inorganic Materials Chemistry, Schuit Institute of Catalysis, Department of Chemical Engineering and Chemistry, Eindhoven University of Technology, 5600 MB Eindhoven, Netherlands; orcid.org/0000-0002-5835-9943

Wei Chen – Laboratory of Inorganic Materials Chemistry, Schuit Institute of Catalysis, Department of Chemical Engineering and Chemistry, Eindhoven University of Technology, 5600 MB Eindhoven, Netherlands

Noortje Donkervoet – Laboratory of Inorganic Materials Chemistry, Schuit Institute of Catalysis, Department of Chemical Engineering and Chemistry, Eindhoven University of Technology, 5600 MB Eindhoven, Netherlands

A. Iulian Dugulan – *Fundamental Aspects of Materials and Energy Group, Delft University of Technology, 2629 JB Delft, Netherlands*

Zhuowu Men – *National Institute of Clean-and-Low-Carbon Energy, Future Science and Technology City, Beijing 102211, People's Republic of China*

Complete contact information is available at:
<https://pubs.acs.org/10.1021/acscatal.1c05634>

Notes

The authors declare no competing financial interest.

■ ACKNOWLEDGMENTS

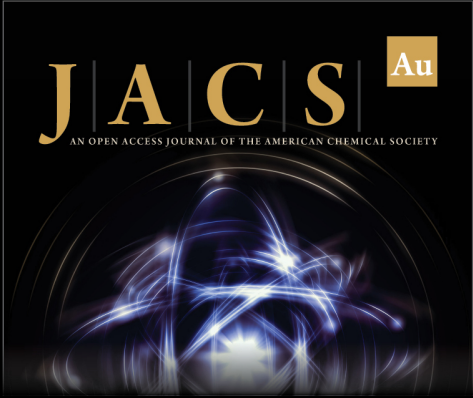
Jiachun Chai acknowledges financial support of the China Scholarship Council. This work was supported by the National Key Research and Development Program of China (no. 2017YFB0602500).

■ REFERENCES

- (1) Fischer, F.; Tropsch, H. Die Erdölsynthese bei gewöhnlichem Druck aus den Vergasungsprodukten der Kohle. *Brennst.-Chem.* **1926**, *7*, 97–104.
- (2) Schulz, H. Short history and present trends of Fischer–Tropsch synthesis. *Appl. Catal. A* **1999**, *186*, 3–12.
- (3) Peña, D.; Cognigni, A.; Neumayer, T.; van Beek, W.; Jones, D. S.; Quijada, M.; Rønning, M. Identification of carbon species on iron-based catalysts during Fischer–Tropsch synthesis. *Appl. Catal., A* **2018**, *554*, 10–23.
- (4) Riedel, T.; Schulz, H.; Schaub, G.; Jun, K.; Hwang, J.; Lee, K. Fischer–Tropsch on iron with H₂/CO and H₂/CO₂ as synthesis gases: the episodes of formation of the Fischer–Tropsch regime and construction of the catalyst. *Top. Catal.* **2003**, *26*, 41–54.
- (5) Davis, B. H. Fischer–Tropsch synthesis: relationship between iron catalyst composition and process variables. *Catal. Today* **2003**, *84*, 83–98.
- (6) Niemantsverdriet, J. W.; van der Kraan, A. M.; Van Dijk, W. L.; Van der Baan, H. S. Behavior of metallic iron catalysts during Fischer–Tropsch synthesis studied with Mössbauer spectroscopy, X-ray diffraction, carbon content determination, and reaction kinetic measurements. *J. Phys. Chem. A* **1980**, *84*, 3363–3370.
- (7) Königer, A.; Hammerl, C.; Zeitler, M.; Rauschenbach, B. Formation of metastable iron carbide phases after high-fluence carbon ion implantation into iron at low temperatures. *Phys. Rev. B* **1997**, *55*, 8143.
- (8) Shroff, M. D.; Kalakkad, D. S.; Coulter, K. E.; Kohler, S. D.; Harrington, M. S.; Jackson, N. B.; Sault, A. G.; Datye, A. K. The importance of passivation in the study of iron Fischer–Tropsch catalysts. *J. Catal.* **1995**, *156*, 185–207.
- (9) Janbroers, S.; Louwen, J. N.; Zandbergen, H. W.; Kooyman, P. J. Insights into the nature of iron-based Fischer–Tropsch catalysts from quasi in situ TEM-EELS and XRD. *J. Catal.* **2009**, *268*, 235–242.
- (10) de Smit, E.; Beale, A. M.; Nikitenko, S.; Weckhuysen, B. M. Local and long range order in promoted iron-based Fischer–Tropsch catalysts: A combined in situ X-ray absorption spectroscopy/wide angle X-ray scattering study. *J. Catal.* **2009**, *262*, 244–256.
- (11) de Smit, E.; Cinquini, F.; Beale, A. M.; Safonova, O. V.; van Beek, W.; Sautet, P.; Weckhuysen, B. M. Stability and reactivity of ϵ - χ - θ Iron carbide catalyst phases in Fischer–Tropsch synthesis: controlling μ_C . *J. Am. Chem. Soc.* **2010**, *132*, 14928–14941.
- (12) Liu, X.; Cao, Z.; Zhao, S.; Gao, R.; Meng, Y.; Zhu, J.; Rogers, C.; Huo, C.; Yang, Y.; Li, Y.; Wen, X. Iron carbides in Fischer–Tropsch synthesis: theoretical and experimental understanding in epsilon-iron carbide phase assignment. *J. Phys. Chem. C* **2017**, *121*, 21390–21396.
- (13) Liu, X.; Zhao, S.; Meng, Y.; Peng, Q.; Dearden, A. K.; Huo, C.; Yang, Y.; Li, Y.; Wen, X. Mössbauer spectroscopy of iron carbides: from prediction to experimental confirmation. *Sci. Rep.* **2016**, *6*, No. 26184.
- (14) Niemantsverdriet, J. W.; van der Kraan, A. M. On the time-dependent behavior of iron catalysts in Fischer–Tropsch synthesis. *J. Catal.* **1981**, *72*, 385–388.
- (15) Mahmoudi, H.; Mahmoudi, M.; Doustdar, O.; Jahangiri, H.; Tsolakis, A.; Gu, S.; Wyszynski, M. A review of Fischer–Tropsch synthesis process, mechanism, surface chemistry and catalyst formulation. *Biofuels Eng.* **2017**, *2*, 11–31.
- (16) Biloen, P.; Helle, J. N.; Sachtler, W. M. H. Incorporation of surface carbon into hydrocarbons during Fischer–Tropsch synthesis: Mechanistic implications. *J. Catal.* **1979**, *58*, 95–107.
- (17) Ekerdt, J. G.; Bell, A. T. Synthesis of hydrocarbons from CO and H₂ over silica-supported Ru: Reaction rate measurements and infrared spectra of adsorbed species. *J. Catal.* **1979**, *58*, 170–187.
- (18) Chen, W.; Pilot, I. A. W.; Pestman, R.; Hensen, E. J. M. Mechanism of cobalt-catalyzed CO hydrogenation: 2. Fischer–Tropsch synthesis. *ACS Catal.* **2017**, *7*, 8061–8071.
- (19) Mars, P.; van Krevelen, D. W. Oxidations carried out by means of vanadium oxide catalysts. *Chem. Eng. Sci.* **1954**, *3*, 41–59.
- (20) Gracia, J. M.; Prinsloo, F. F.; Niemantsverdriet, J. W. Mars-van Krevelen-like mechanism of CO hydrogenation on an iron carbide surface. *Catal. Lett.* **2009**, *133*, 257–261.
- (21) Kummer, J. T.; DeWitt, T. W.; Emmett, P. H. Some mechanism studies on the Fischer–Tropsch synthesis using C¹⁴. *J. Am. Chem. Soc.* **1948**, *70*, 3632–3643.
- (22) Ordonsky, V. V.; Legras, B.; Cheng, K.; Paul, S.; Khodakov, A. Y. The role of carbon atoms of supported iron carbides in Fischer–Tropsch synthesis. *Catal. Sci. Technol.* **2015**, *5*, 1433–1437.
- (23) Wang, P.; Chen, W.; Chiang, F.; Dugulan, A. I.; Song, Y.; Pestman, R.; Zhang, K.; Yao, J.; Feng, B.; Miao, P.; Xu, W.; Hensen, E. J. M. Synthesis of stable and low-CO₂ selective ϵ -iron carbide Fischer–Tropsch catalysts. *Sci. Adv.* **2018**, *4*, No. eaau2947.
- (24) Chen, W.; Pestman, R.; Zijlstra, B.; Pilot, I. A. W.; Hensen, E. J. M. Mechanism of cobalt-catalyzed CO hydrogenation: 1. Methanation. *ACS Catal.* **2017**, *7*, 8050–8060.
- (25) Chai, J.; Pestman, R.; Chen, W.; Dugulan, A. I.; Feng, B.; Men, Z.; Wang, P.; Hensen, E. J. M. The role of H₂ in Fe carburization by CO in Fischer–Tropsch catalysts. *J. Catal.* **2021**, *400*, 93–102.
- (26) Xu, J.; Bartholomew, C. H. Temperature-programmed hydrogenation (TPH) and *in situ* Mössbauer Spectroscopy studies of carbonaceous species on silica-supported iron Fischer–Tropsch catalysts. *J. Phys. Chem. B* **2005**, *109*, 2392–2403.
- (27) Rao, K. R. P. M.; Huggins, F. E.; Huffman, G. P.; Gormley, R. J.; O'Brien, R. J.; Davis, B. H. Mössbauer study of iron Fischer–Tropsch catalysts during activation and synthesis. *Energy Fuels* **1996**, *10*, 546–551.
- (28) Ojeda, M.; Nabar, R.; Nilekar, A. U.; Ishikawa, A.; Mavrikakis, M.; Iglesia, E. CO activation pathways and the mechanism of Fischer–Tropsch synthesis. *J. Catal.* **2010**, *272*, 287–297.
- (29) Sorescu, D. C. First-principles calculations of the adsorption and hydrogenation reactions of CH_x (x = 0, 4) species on a Fe (100) surface. *Phys. Rev. B* **2006**, *73*, No. 1554207.
- (30) Govender, N. S.; Botes, F. G.; de Croon, M. H. J. M.; Schouten, J. C. Mechanistic pathway for methane formation over an iron-based catalyst. *J. Catal.* **2008**, *260*, 254–261.
- (31) Shannon, S. L.; Goodwin, J. G. Characterization of catalytic surfaces by isotopic-transient kinetics during steady-state reaction. *Chem. Rev.* **1995**, *95*, 677–695.
- (32) de Pontes, M.; Yokomizo, G. H.; Bell, A. T. Novel method for analyzing transient response data obtained in isotopic tracer studies of CO hydrogenation. *J. Catal.* **1987**, *104*, 147–155.
- (33) Biloen, P. Transient kinetic methods. *J. Mol. Catal.* **1983**, *21*, 17–24.
- (34) Eddy Hoost, T.; Goodwin, J. G. Nonparametric determination of reactivity distributions from isotopic transient kinetic data. *J. Catal.* **1992**, *134*, 678–690.


(35) Graf, B.; Schulte, H.; Muhler, M. The formation of methane over iron catalysts applied in Fischer–Tropsch synthesis: A transient and steady state kinetic study. *J. Catal.* **2010**, *276*, 66–75.


(36) Govender, N. S.; Botes, F. G.; de Croon, M. H. J. M.; Schouten, J. C. Mechanistic pathway for C₂+ hydrocarbons over an Fe/K catalyst. *J. Catal.* **2014**, *312*, 98–107.




The image shows the front cover of the journal JACS Au. The title "JACS Au" is prominently displayed in a gold serif font, with "Au" in a separate gold box. Below the title, it says "AN OPEN ACCESS JOURNAL OF THE AMERICAN CHEMICAL SOCIETY". The central graphic is an abstract, glowing blue and white molecular or atomic structure. Below the graphic is a small portrait of Prof. Christopher W. Jones, followed by his name and title: "Editor-in-Chief Prof. Christopher W. Jones, Georgia Institute of Technology, USA". A large gold banner at the bottom reads "Open for Submissions" with a gold padlock icon. At the very bottom, the website "pubs.acs.org/jacsau" is on the left, and the ACS Publications logo with the tagline "Most Trusted. Most Cited. Most Read." is on the right.

JACS Au
AN OPEN ACCESS JOURNAL OF THE AMERICAN CHEMICAL SOCIETY

 Editor-in-Chief
Prof. Christopher W. Jones
Georgia Institute of Technology, USA

Open for Submissions 

pubs.acs.org/jacsau  **ACS Publications**
Most Trusted. Most Cited. Most Read.